Disturbance Observer-Based Fast Fixed-Time Nonsingular Terminal Sliding-Mode Formation Control for Autonomous Underwater Vehicles

Hongde Qin, Jinshuai Si(✉), and Liyang Gao

Harbin Engineering University, Harbin 150001, China
sijinshuai0820@163.com

Abstract. In this paper, a disturbance observer-based fixed-time formation control method is studied for autonomous underwater vehicles with actuator faults, model uncertainties and external disturbances. Firstly, the leader-follower strategy is combined with the artificial potential field method to obtain the formation configuration. Then, a fast fixed-time disturbance observer is designed to deal with unknown composite disturbances. Further, based on the disturbance observer and fixed-time nonsingular terminal sliding-mode surface, a novel fast fixed-time formation control method is proposed. Finally, simulation results show the effectiveness of the proposed method.

Keywords: Autonomous underwater vehicles · Formation control · Nonsingular fixed-time terminal sliding-mode · Fixed-time disturbance observer

1 Introduction

In the past decade, autonomous underwater vehicles (AUV) have attracted wide attention due to its outstanding performance in underwater oil exploration, underwater surveillance and minesweeping. When performing tasks, the team cooperation of multiple AUVs is often more efficient than that of a single AUV. At the same time, in order to complete the task efficiently, advanced control methods are crucial [1–3]. Therefore, it is essential to study the formation control of AUVs. The common formation methods of AUV include leader-follower method [4], behavior-based method [5], artificial potential field method [6] and virtual structure [7], which the leader-follower method is the most widely used [8, 9]. Since different control methods have their own different advantages, two different formation control methods can be combined to enhance their respective advantages. In [10], Wu proposed a control method combining artificial potential field (APF) and leader-follower, which achieved the desired formation structure without collision.

In order to ensure fast and accurate control effect, the sliding mode control (SMC) is often used [11–18]. The traditional sliding mode control can only guarantee the asymptotic stability or finite-time stability of the system, which the convergence time cannot be calculated [19]. In [20], Polyakov proposed fixed-time control for the first time, which can make the system stable in a fixed time without considering the initial conditions.

H. R. Karimi and N. Wang (Eds.): S-Cube 2022, LNICST 487, pp. 146–163, 2023.
https://doi.org/10.1007/978-3-031-34899-0_10

In [21], two fixed-time formation control methods for multi-robot formation systems with undirected topology and directed topology were presented. In [22], a new control algorithm based on fixed-time control and switching control method was presented for multi-agent systems with first-order and second-order dynamic models, which can achieve the distributed consensus for multi-agent in a fixed time.

The multi-AUV formation system is susceptible to external disturbances and the unmodeled dynamics of the system, which poses a huge challenge to achieve stable formation effect [23]. At present, the main methods to cope with disturbances include neural network and disturbance observer [24–32]. Based on the study of traditional nonlinear disturbance observer, a disturbance estimator is used in formation control method to achieve accurately estimation of disturbances. In [33], a fixed-time disturbance estimator was proposed for USV systems with actuator saturation and dead zone, which can accurately estimate unknown disturbances. In [34], a fixed-time integral sliding-mode disturbance estimator was devised to deal with disturbances, which greatly improved the robustness of the system and was not limited by the initial conditions of the system.

Driven by the above observations, we design a multi-AUV formation control algorithm based on a fixed-time disturbance observer considering actuator fault, model uncertainties and unknown disturbances. Firstly, the desired formation configuration is obtained by combining leader-follower and APF. Then, actuator fault, unmodeled dynamics and unknown disturbances are considered as composite disturbances, and a fixed time disturbance observer is proposed to estimate them accurately. Finally, based on the fixed-time theory and sliding-mode control, a novel formation control method is proposed, which realizes the desired formation structure in a fixed time. The contributions of this article are summarized as follows:

(1) By combining the leader-follower with artificial potential field strategy, the desired formation configuration can be obtained.
(2) A fixed-time disturbance observer is designed to cope with complex disturbances, which enhances the robustness of the entire system.
(3) A new fixed-time formation control method is presented based on a fixed-time nonsingular terminal sliding-mode surface, which reaches the formation configuration.

2 Preliminaries and Problem Formulation

2.1 Preliminaries

Lemma 1. Inspired by [35], if the following system satisfies

$$\dot{z} = -\frac{1}{N(z)}\left(\alpha_0 \boldsymbol{sig}^{1+\kappa}(z) + \beta_0 \boldsymbol{sig}^{\frac{p}{q}}(z)\right) \tag{1}$$

where $\kappa = \left(\frac{m}{2n}\right)(1 + \mathrm{sgn}(|z| - 1))$. $\alpha_0 > 0$, $\beta_0 > 0$, $0 < a < 1$, $b > 0$ are four scalars. $c > 0$ is an even integer. $m > 0$, $n > 0$, $p > 0$, $q > 0$ are odd integers satisfying $m > n$, $p < q$ and $N(z) = a + (1 - a)\exp\left(-b|z|^c\right)$, $\begin{cases} c, & |z| \geq 1 \\ 1, & |z| < 1 \end{cases}$. The convergence time of the system is

$$T < \frac{n}{\alpha_0 m} + \frac{q}{\alpha_0(q-p)} \ln\left(1 + \frac{\alpha_0}{\beta_0}\right) \tag{2}$$

Remark 1. Compared with [35], the fixed-time stable system has faster convergence performance. In detail, the $N(z)$ is smaller than the $N(z)$ proposed in [35] when $|z| < 1$, which means that when the state of the system approaches the equilibrium point, the convergence rate is improved. Therefore, it is demonstrated that the system is faster than [35].

2.2 Problem Formulation

2.2.1 Leader-Follower Strategy Based on APF.

Considering the formation configuration, we choose the leader-follower strategy based on APF. The position information of i-th AUV relative to the leader l is

$$\dot{\boldsymbol{\eta}}_i - \dot{\boldsymbol{\eta}}_l = -\nabla_{\eta i}\boldsymbol{J}(\boldsymbol{\eta}) \tag{3}$$

where $\boldsymbol{\eta}_l$ is the position information of the leader. The net potential function is denoted as $\boldsymbol{J}(\boldsymbol{\eta})$, which represents the interaction between AUVs and it is shown as

$$\boldsymbol{J}(\boldsymbol{\eta}) = \sum_{i=1}^{N} \boldsymbol{J}_a\big(\|\boldsymbol{\eta}_i - \boldsymbol{\eta}_l\|\big) - \boldsymbol{J}_r\big(\|\boldsymbol{\eta}_i - \boldsymbol{\eta}_l\|\big) \tag{4}$$

where $\boldsymbol{J}_a(\bullet)$ denotes the attractive potential field and $\boldsymbol{J}_r(\bullet)$ denotes the repulsive potential field. The formation configuration is restricted by artificial potential field. $\boldsymbol{J}_a(\bullet)$ and $\boldsymbol{J}_r(\bullet)$ are shown as

$$\boldsymbol{J}_a(\bullet) = \frac{1}{2}a\|\bullet\|^2 \tag{5}$$

$$\boldsymbol{J}_r(\bullet) = -\frac{1}{2}bc\exp\left(-\frac{\|\bullet\|^2}{c}\right) \tag{6}$$

where a, b, c are three constants, which are relevant to the distance between the follower and the leader. In this paper, when $\|\boldsymbol{\eta}_i - \boldsymbol{\eta}_l\| = d$ and $\boldsymbol{J}_a(\bullet) = \boldsymbol{J}_r(\bullet)$ are satisfied, the unique minimum value is obtained. Meanwhile, the net gradient potential field is zero, and the formation configuration is realized. The potential field gradient is shown as

$$\nabla\boldsymbol{J}_a(\bullet) = a\big(\boldsymbol{\eta}_i - \boldsymbol{\eta}_l\big)\big/\,\big\|\big(\boldsymbol{\eta}_i - \boldsymbol{\eta}_l\big)\big\| \tag{7}$$

$$\nabla\boldsymbol{J}_r(\bullet) = -\left[b\big(\boldsymbol{\eta}_i - \boldsymbol{\eta}_j\big) \times \boldsymbol{e}^{-\|\boldsymbol{\eta}_i - \boldsymbol{\eta}_j\|^2/c}\right] \tag{8}$$

$$\nabla_{\eta i}\boldsymbol{J}(\bullet) = \nabla\boldsymbol{J}_a(\bullet) + \nabla\boldsymbol{J}_r(\bullet) \tag{9}$$

where $\nabla\boldsymbol{J}_a(\bullet)$ is the attractive force to reach formation configuration and $\nabla\boldsymbol{J}_r(\bullet)$ represents the repulsive force to avoid collision.

2.2.2 AUV Dynamics

The kinematics and dynamics equations of i-th AUV are shown as

$$\dot{\boldsymbol{\eta}}_i = \boldsymbol{R}(\psi_i)\boldsymbol{v}_i \tag{10}$$

$$\boldsymbol{M}_i\dot{\boldsymbol{v}}_i + \boldsymbol{C}(\boldsymbol{v}_i)\boldsymbol{v}_i + \boldsymbol{D}(\boldsymbol{v}_i)\boldsymbol{v}_i = \boldsymbol{\tau}_i + \boldsymbol{\tau}_{di} \tag{11}$$

where $\boldsymbol{\eta_i} = \left[x_i,\ y_i,\ \psi_i\right]^{\mathrm{T}}$ represents the position information, $\boldsymbol{v_i} = [u_i,\ v_i,\ r_i]^{\mathrm{T}}$ represents the velocity information, $\boldsymbol{M}_i$, $\boldsymbol{C}(v_i)$ and $\boldsymbol{D}(v_i)$ represent inertia matrix, Coriolis matrix and damping matrix, respectively. $\boldsymbol{\tau}_i = [\tau_{iu},\ \tau_{iv},\ \tau_{ir}]^{\mathrm{T}}$ denotes control inputs, $\boldsymbol{\tau}_{di}$ indicates external disturbance. $\boldsymbol{R}(\psi_i)$ represents the rotation matrix and is expressed as $\boldsymbol{R}(\psi_i) = \begin{bmatrix} \cos(\psi_i) & -\sin(\psi_i) & 0 \\ \sin(\psi_i) & \cos(\psi_i) & 0 \\ 0 & 0 & 1 \end{bmatrix}$. $\boldsymbol{R}^{\mathrm{T}}(\psi_i)\boldsymbol{R}(\psi_i) = \boldsymbol{I}$, $\dot{\boldsymbol{R}}(\psi_i) = \boldsymbol{R}(\psi_i)\boldsymbol{S}(r)$, $\forall\psi_i \subseteq [0,\ 2\pi]$, and $\boldsymbol{R}^{\mathrm{T}}(\psi_i)\boldsymbol{S}(r)\boldsymbol{R}(\psi_i) = \boldsymbol{R}(\psi_i)\boldsymbol{S}(r)\boldsymbol{R}^{\mathrm{T}}(\psi_i) = \boldsymbol{S}(r)$, where $\boldsymbol{S}(r) = \begin{bmatrix} 0 & -r & 0 \\ r & 0 & 0 \\ 0 & 0 & 0 \end{bmatrix}$

For actuator faults, the control input $\boldsymbol{\tau}_i$ is defined as

$$\boldsymbol{\tau}_i = \boldsymbol{\tau}_{Ai} + [(\boldsymbol{E}(t) - \boldsymbol{I})\boldsymbol{\tau}_{Ai} + \overline{\boldsymbol{\tau}}_i] = \boldsymbol{\tau}_{Ai} + \boldsymbol{\tau}_{Fi} \tag{12}$$

where $\boldsymbol{\tau}_{Ai}$ is the actual control input and $\overline{\boldsymbol{\tau}}_i$ is the additional bias fault. $\boldsymbol{E}(t) = \mathrm{diag}\{\mathrm{e}_1,\ \mathrm{e}_2,\ \mathrm{e}_3\}$ indicates the effective coefficient matrix of the actuator. When $e_i = 1$ and $\overline{\boldsymbol{\tau}}_i = 0$, it represents that the actuator is working normally; when $e_i = 0$, it represents that the actuator is working normally. In this paper, $e_i > 1$ is considered.

According to Eqs. (10)–(12), the model is written as

$$\boldsymbol{M}_{\eta i}\left(\boldsymbol{\eta}_i\right)\ddot{\boldsymbol{\eta}}_i + \boldsymbol{C}_{\eta i}\left(\boldsymbol{\eta}_i,\ \dot{\boldsymbol{\eta}}_i\right)\dot{\boldsymbol{\eta}}_i + \boldsymbol{D}_{\eta i}\left(\boldsymbol{\eta}_i,\ \dot{\boldsymbol{\eta}}_i\right)\dot{\boldsymbol{\eta}}_i = \boldsymbol{\tau}_{\eta i} + \boldsymbol{R}(\psi_i)\boldsymbol{\tau}_{di} + \boldsymbol{R}(\psi_i)\boldsymbol{\tau}_{Fi} \tag{13}$$

where $\boldsymbol{M}_{\eta i}\left(\boldsymbol{\eta}_i\right) = \boldsymbol{R}(\psi_i)\boldsymbol{M}_i\boldsymbol{R}^{\mathrm{T}}(\psi_i)$, $\boldsymbol{C}_{\eta i}\left(\boldsymbol{\eta}_i,\ \dot{\boldsymbol{\eta}}_i\right)$=$\boldsymbol{R}(\psi_i)(\boldsymbol{C}_i - \boldsymbol{M}_i\boldsymbol{S})\boldsymbol{R}^{\mathrm{T}}(\psi_i)$, $\boldsymbol{\tau}_{\eta i} = \boldsymbol{R}(\psi_i)\boldsymbol{\tau}_{Ai}$, $\boldsymbol{D}_{\eta i}\left(\boldsymbol{\eta}_i,\ \dot{\boldsymbol{\eta}}_i\right) = \boldsymbol{R}(\psi_i)\boldsymbol{D}_i\boldsymbol{R}^{\mathrm{T}}(\psi_i)$.

In general, accurate model parameters are often unavailable. Therefore, the parameter matrix can be divided into two parts.

$$\boldsymbol{M}_{\eta i}\left(\boldsymbol{\eta}_i\right) = \hat{\boldsymbol{M}}_{\eta i}\left(\boldsymbol{\eta}_i\right) + \Delta\boldsymbol{M}_{\eta i}\left(\boldsymbol{\eta}_i\right) \tag{14}$$

$$\boldsymbol{C}_{\eta i}\left(\boldsymbol{\eta}_i,\ \dot{\boldsymbol{\eta}}_i\right) = \hat{\boldsymbol{C}}_{\eta i}\left(\boldsymbol{\eta}_i,\ \dot{\boldsymbol{\eta}}_i\right) + \Delta\boldsymbol{C}_{\eta i}\left(\boldsymbol{\eta}_i,\ \dot{\boldsymbol{\eta}}_i\right) \tag{15}$$

$$\boldsymbol{D}_{\eta i}\left(\boldsymbol{\eta}_i,\ \dot{\boldsymbol{\eta}}_i\right) = \hat{\boldsymbol{D}}_{\eta i}\left(\boldsymbol{\eta}_i,\ \dot{\boldsymbol{\eta}}_i\right) + \Delta\boldsymbol{D}_{\eta i}\left(\boldsymbol{\eta}_i,\ \dot{\boldsymbol{\eta}}_i\right) \tag{16}$$

where $\hat{\boldsymbol{M}}_{\eta i}\left(\boldsymbol{\eta}_i\right)$, $\hat{\boldsymbol{C}}_{\eta i}\left(\boldsymbol{\eta}_i,\ \dot{\boldsymbol{\eta}}_i\right)$, and $\hat{\boldsymbol{D}}_{\eta i}\left(\boldsymbol{\eta}_i,\ \dot{\boldsymbol{\eta}}_i\right)$ represent the nominal terms and $\Delta\boldsymbol{M}_{\eta i}\left(\boldsymbol{\eta}_i\right)$, $\Delta\boldsymbol{C}_{\eta i}\left(\boldsymbol{\eta}_i,\ \dot{\boldsymbol{\eta}}_i\right)$, $\Delta\boldsymbol{D}_{\eta i}\left(\boldsymbol{\eta}_i,\ \dot{\boldsymbol{\eta}}_i\right)$ represent the uncertain terms.

Through the above equations, we get

$$\hat{\boldsymbol{M}}_{\eta i}\left(\boldsymbol{\eta}_i\right)\ddot{\boldsymbol{\eta}}_i + \hat{\boldsymbol{C}}_{\eta i}\left(\boldsymbol{\eta}_i,\ \dot{\boldsymbol{\eta}}_i\right)\dot{\boldsymbol{\eta}}_i + \hat{\boldsymbol{D}}_{\eta i}\left(\boldsymbol{\eta}_i,\ \dot{\boldsymbol{\eta}}_i\right)\dot{\boldsymbol{\eta}}_i = \boldsymbol{\tau}_{\eta i} + \boldsymbol{d'}_i \tag{17}$$

where $\boldsymbol{d'}_i$ represents the uncertainty of the lumped system

$$\boldsymbol{d'}_i = \boldsymbol{R}(\psi_i)\boldsymbol{\tau}_{di} + \boldsymbol{R}(\psi_i)\boldsymbol{\tau}_{Fi} - \Delta\boldsymbol{M}_{\eta i}(\boldsymbol{\eta}_i)\ddot{\boldsymbol{\eta}}_i - \Delta\boldsymbol{C}_{\eta i}(\boldsymbol{\eta}_i, \dot{\boldsymbol{\eta}}_i)\dot{\boldsymbol{\eta}}_i - \Delta\boldsymbol{D}_{\eta i}(\boldsymbol{\eta}_i, \dot{\boldsymbol{\eta}}_i)\dot{\boldsymbol{\eta}}_i \quad (18)$$

Consider the desired position information $\boldsymbol{\eta}_i^d = \boldsymbol{\eta}_l - \int_0^t \nabla_{\eta i}\boldsymbol{J}(\boldsymbol{\eta})$ and define the formation position error $\boldsymbol{\eta}_{ei} = \boldsymbol{\eta}_i - \boldsymbol{\eta}_i^d$ and auxiliary error $\boldsymbol{\omega}_{ei} = \dot{\boldsymbol{\eta}}_i - \dot{\boldsymbol{\eta}}_i^d$. Therefore, let $\boldsymbol{x}_{1i} = \boldsymbol{\eta}_{ei}$, $\boldsymbol{x}_{2i} = \boldsymbol{\omega}_{ei}$, the kinematics and dynamics equations can be modified as

$$\begin{cases} \dot{\boldsymbol{x}}_{1i} = \boldsymbol{x}_{2i} \\ \dot{\boldsymbol{x}}_{2i} = \boldsymbol{u}_i + \boldsymbol{d}_i - \hat{\boldsymbol{M}}_{\eta i}^{-1}(\boldsymbol{\eta}_i)\left(\hat{\boldsymbol{C}}_{\eta i}(\boldsymbol{\eta}_i, \dot{\boldsymbol{\eta}}_i)\dot{\boldsymbol{\eta}}_i + \hat{\boldsymbol{D}}_{\eta i}(\boldsymbol{\eta}_i, \dot{\boldsymbol{\eta}}_i)\dot{\boldsymbol{\eta}}_i\right) - \ddot{\boldsymbol{\eta}}_i^d \end{cases} \quad (19)$$

where $\boldsymbol{u}_i = \hat{\boldsymbol{M}}_{\eta i}^{-1}(\boldsymbol{\eta}_i)\boldsymbol{\tau}_{\eta i}$ is transformed control input, $\boldsymbol{d}_i = \hat{\boldsymbol{M}}_{\eta i}^{-1}(\boldsymbol{\eta}_i)\boldsymbol{d'}_i$ is composite disturbance.

3 Main Results

The composite disturbance and the convergence rate of the system will affect the efficiency of formation task. In order to improve the efficiency of formation task, a new fixed-time formation control method is proposed by combining a fixed-time observer with the improved sliding-mode surface, which is also the main result of this paper.

3.1 Fixed-Time Disturbance Observer Design and Analysis

The existence of composite disturbance will affect the state of the system. If we cannot deal with the composite disturbance well, it will have a negative impact on the formation result. Therefore, in order to ensure that the system has good performance in the presence of composite disturbance, a new fixed-time disturbance observer is designed to estimate this composite disturbance $\boldsymbol{d}_i$ in this part. An auxiliary system is designed as

$$\boldsymbol{x}_{fi} = \gamma_1 \int_0^t \left[\boldsymbol{u}_i - \hat{\boldsymbol{M}}_{\eta i}^{-1}(\boldsymbol{\eta}_i)\left(\hat{\boldsymbol{C}}_{\eta i}(\boldsymbol{\eta}_i, \dot{\boldsymbol{\eta}}_i)\dot{\boldsymbol{\eta}}_i + \hat{\boldsymbol{D}}_{\eta i}(\boldsymbol{\eta}_i, \dot{\boldsymbol{\eta}}_i)\dot{\boldsymbol{\eta}}_i\right) - \ddot{\boldsymbol{\eta}}_i^d - \boldsymbol{x}_{fi}\right] d\tau - \gamma_1 \boldsymbol{x}_{2i} \quad (20)$$

where $\boldsymbol{x}_{fi}$ is the auxiliary system, and $\gamma_1 > 0$ is the control parameter. Taking the derivative of (20), we get

$$\dot{\boldsymbol{x}}_{fi} = -\gamma_1 \boldsymbol{x}_{fi} - \gamma_1 \boldsymbol{d}_i \quad (21)$$

$$\boldsymbol{y}_{1i} = \gamma_2 \boldsymbol{x}_{fi} \quad (22)$$

where y_{1i} denotes the output of (22) and $\gamma_2 > 0$ denotes a gain parameter.

The estimation of $\boldsymbol{x}_{fi}$ is designed as $\hat{\boldsymbol{x}}_{fi}$

$$\dot{\hat{\boldsymbol{x}}}_{fi} = -\gamma_3\gamma_2\hat{\boldsymbol{x}}_{fi} + \gamma_2^{-1}\dot{\boldsymbol{y}}_{1i} + \gamma_3\boldsymbol{y}_{1i} + \frac{1}{N(\tilde{\boldsymbol{x}}_{fi})}\left(\lambda_1 \boldsymbol{sig}^{k_1}(\tilde{\boldsymbol{x}}_{fi}) + \lambda_2 \boldsymbol{sig}^{k_2}(\tilde{\boldsymbol{x}}_{fi})\right) \quad (23)$$

where $\tilde{\boldsymbol{x}}_{fi} = \boldsymbol{x}_{fi} - \hat{\boldsymbol{x}}_{fi}$ is estimation error, and $\gamma_3 > 0$ is a control gain parameter. $N(\tilde{\boldsymbol{x}}_{fi}) = a_1 + (1-a_1)\exp\left(-b_1|\tilde{\boldsymbol{x}}_{fi}|^{c_1}\right), \begin{cases} c_1, & |\tilde{\boldsymbol{x}}_{fi}| \geq 1 \\ 1, & |\tilde{\boldsymbol{x}}_{fi}| < 1 \end{cases}, k_1 = 1 + \left(\frac{m_1}{2n_1}\right)\left(1 + \mathrm{sgn}\left(|\tilde{\boldsymbol{x}}_{fi}| - 1\right)\right), k_2 = \frac{p_1}{q_1}$, $\lambda_1 > 0$, $\lambda_2 > 0$, $0 < a_1 < 1$, $b_1 > 0$, $c_1 > 0$ are five constants. $m_1 > n_1 > 0$, $0 < p_1 < q_1$ are four odd integers.

Lemma 2. Based on the proposed auxiliary system (20), the estimation error will converge to the origin in a fixed time, and the convergence time T_0 is

$$T_0 < \frac{1}{\lambda_1 \mu_1} + \frac{1}{\lambda_1(1-\omega_1)} \ln\left(1 + \frac{\lambda_1}{2^{(\omega_1-1)/2}\lambda_2}\right) \tag{24}$$

where $\mu_1 = \frac{m_1}{n_1}$, $\omega_1 = \frac{p_1}{q_1}$.

Proof. Consider the Lyapunov function $V_1 = \frac{1}{2}\tilde{\boldsymbol{x}}_{fi}^{\mathrm{T}}\tilde{\boldsymbol{x}}_{fi}$, and the derivative of V_1 satisfies

$$\begin{aligned}
\dot{V}_1 &= \tilde{\boldsymbol{x}}_{fi}^{\mathrm{T}}\dot{\tilde{\boldsymbol{x}}}_{fi} = \tilde{\boldsymbol{x}}_{fi}^{\mathrm{T}}\left(\dot{\boldsymbol{x}}_{fi} - \dot{\hat{\boldsymbol{x}}}_{fi}\right) \\
&= \tilde{\boldsymbol{x}}_{fi}^{\mathrm{T}}\left(-\gamma_1 \boldsymbol{x}_{fi} - \gamma_1 \boldsymbol{d}_i + \gamma_3\gamma_2\hat{\boldsymbol{x}}_{fi} - \gamma_2^{-1}\gamma_2\boldsymbol{x}_{fi} - \gamma_3\gamma_2\boldsymbol{x}_{fi}\right) \\
&\quad - \tilde{\boldsymbol{x}}_{fi}^{\mathrm{T}}\frac{1}{N(\tilde{\boldsymbol{x}}_{fi})}\left(\lambda_1 \boldsymbol{sig}^{k_1}(\tilde{\boldsymbol{x}}_{fi}) + \lambda_2 \boldsymbol{sig}^{k_2}(\tilde{\boldsymbol{x}}_{fi})\right) \\
&= \tilde{\boldsymbol{x}}_{fi}^{\mathrm{T}}\left(-\gamma_3\gamma_2\tilde{\boldsymbol{x}}_{fi} - \frac{1}{N(\tilde{\boldsymbol{x}}_{fi})}\left(\lambda_1 \boldsymbol{sig}^{k_1}(\tilde{\boldsymbol{x}}_{fi}) + \lambda_2 \boldsymbol{sig}^{k_2}(\tilde{\boldsymbol{x}}_{fi})\right)\right) \\
&\leq -\tilde{\boldsymbol{x}}_{fi}^{\mathrm{T}}\frac{1}{N(\tilde{\boldsymbol{x}}_{fi})}\left(\lambda_1 \boldsymbol{sig}^{k_1}(\tilde{\boldsymbol{x}}_{fi}) + \lambda_2 \boldsymbol{sig}^{k_2}(\tilde{\boldsymbol{x}}_{fi})\right) \\
&\leq -\sum_{j=1}^{3}\frac{1}{N(\tilde{\boldsymbol{x}}_{fi,j})}\left(\lambda_1|\tilde{\boldsymbol{x}}_{fi,j}|^{k_1+1} + \lambda_2|\tilde{\boldsymbol{x}}_{fi,j}|^{k_2+1}\right) \\
&\leq -\frac{1}{N(\tilde{\boldsymbol{x}}_{fi})}\lambda_1(2V_1)^{(k_1+1)/2} - \frac{1}{N(\tilde{\boldsymbol{x}}_{fi})}\lambda_2(2V_1)^{(k_2+1)/2}
\end{aligned} \tag{25}$$

when $|\tilde{\boldsymbol{x}}_{fi}| \geq 1$, one has

$$\dot{V}_1 \leq -\frac{1}{N(\tilde{\boldsymbol{x}}_{fi})}\lambda_1(2V_1)^{(\mu_1+1)/2} - \frac{1}{N(\tilde{\boldsymbol{x}}_{fi})}\lambda_2(2V_1) \tag{26}$$

when $|\tilde{\boldsymbol{x}}_{fi}| < 1$, one has

$$\dot{V}_1 \leq -\frac{1}{N(\tilde{\boldsymbol{x}}_{fi})}\lambda_1(2V_1) - \frac{1}{N(\tilde{\boldsymbol{x}}_{fi})}\lambda_2(2V_1)^{(\omega_1+1)/2} \tag{27}$$

Therefore, the error of the auxiliary system can converge to the origin in a fixed time.

$$T_0 < \frac{1}{\lambda_1 \mu_1} + \frac{1}{\lambda_1(1-\omega_1)} \ln\left(1 + \frac{\lambda_1}{2^{(\omega_1-1)/2}\lambda_2}\right) \tag{28}$$

Lemma 3. The estimated value of composite disturbance is defined as

$$\hat{\boldsymbol{d}}_i = -(\gamma_1\gamma_2)^{-1}\dot{\boldsymbol{y}}_{1i} - \hat{\boldsymbol{x}}_{fi} \tag{29}$$

Proof. Define the error $\tilde{\boldsymbol{d}}_i = \hat{\boldsymbol{d}}_i - \boldsymbol{d}_i$. From (22), we have

$$\boldsymbol{d}_i = -\boldsymbol{x}_{fi} - \gamma_1^{-1}\dot{\boldsymbol{x}}_{fi} \tag{30}$$

Then, combining Eqs. (29) and (30), we can further get

$$\begin{aligned}\tilde{\boldsymbol{d}}_i = \hat{\boldsymbol{d}}_i - \boldsymbol{d}_i &= -(\gamma_1\gamma_2)^{-1}\dot{\boldsymbol{y}}_{1i} - \hat{\boldsymbol{x}}_{fi} + \boldsymbol{x}_{fi} + \gamma_1^{-1}\dot{\boldsymbol{x}}_{fi} \\ &= -\gamma_1^{-1}\dot{\boldsymbol{x}}_{fi} + \gamma_1^{-1}\dot{\boldsymbol{x}}_{fi} - \hat{\boldsymbol{x}}_{fi} + \boldsymbol{x}_{fi} = \tilde{\boldsymbol{x}}_{fi}\end{aligned} \tag{31}$$

According to Lemma 2, we can obtain that $\tilde{\boldsymbol{d}}_i$ tends to 0 for $t \geq T_0$. Therefore, the composite disturbance can accurately be observed by the proposed fixed-time disturbance observer. This means that the robustness of the system is greatly enhanced.

Remark 2. The proposed fixed-time disturbance observer in this part has the following advantages. On the one hand, the convergence rate of the observation error is improved, and the convergence time of the system is not affected by the initial conditions. On the other hand, we can observe the composite disturbance accurately without knowing prior information about it, which means that the observer can be better applied in practice.

3.2 Nonsingular Fast Fixed-Time Controller Design

The convergence rate is a very important performance index in the control system. The faster convergence rate can accomplish the formation task more efficiently. Therefore, based on the above analysis, a novel nonsingular fast fixed-time formation controller is designed.

Inspired by Lemma 1, the sliding-mode surface is designed as

$$\boldsymbol{S}_i = \boldsymbol{x}_{2i} + \frac{1}{N(\boldsymbol{x}_{1i})}\left(\lambda_3 \boldsymbol{sig}^{k_3}(\boldsymbol{x}_{1i}) + \lambda_4 \boldsymbol{S}_{ci}\right) \tag{32}$$

where $\boldsymbol{S}_{i,j} = \left[S_{i,1}, S_{i,2}, S_{i,3}\right]^{\mathrm{T}}$, $N(x_{1i}) = a_2 + (1-a_2)\exp\left(-b_2|\boldsymbol{x}_{1i}|^{c_2}\right)$, $\begin{cases} c_2, & |\boldsymbol{x}_{1i}| \geq 1 \\ 1, & |\boldsymbol{x}_{1i}| < 1 \end{cases}$, and $k_3 = 1 + \left(\frac{m_2}{2n_2}\right)(1 + \mathrm{sgn}(|\boldsymbol{x}_{1i}| - 1))$. $\lambda_3 > 0$, $\lambda_4 > 0$, $0 < a_2 < 1$, $b_2 > 0$ are four scalars. $c_2 > 0$ is an even integer. $m_2 > n_2 > 0$ are two odd integers. $\boldsymbol{S}_{ci,j} = \left[S_{ci,1}, S_{ci,2}, S_{ci,3}\right]^{\mathrm{T}}$ is designed as

$$\boldsymbol{S}_{ci} = \begin{cases} \boldsymbol{sig}^{k_4}(\boldsymbol{x}_{1i}), & \text{if } \overline{\boldsymbol{S}}_i = 0 \text{ or } \overline{\boldsymbol{S}}_i \neq 0,\ |\boldsymbol{x}_{1i}| \geq \phi \\ \sigma_1 \boldsymbol{x}_{1i} + \sigma_2 \boldsymbol{x}_{1i}^2 \mathrm{sgn}(\boldsymbol{x}_{1i}), & \text{if } \overline{\boldsymbol{S}}_i \neq 0,\ |\boldsymbol{x}_{1i}| < \phi \end{cases} \tag{33}$$

where $k_4 = \frac{p_2}{q_2}, 0 < \phi < 1.0 < p_2 < q_2$ are two odd integers and $\sigma_1 = \left(2 - \frac{p_2}{q_2}\right)\phi^{\frac{p_2}{q_2}-1}$, $\sigma_2 = \left(\frac{p_2}{q_2} - 1\right)\phi^{\frac{p_2}{q_2}-2}$, $\overline{\boldsymbol{S}}_i = \boldsymbol{x}_{2i} + \frac{1}{N(\boldsymbol{x}_{1i})}\left(\lambda_3 \boldsymbol{sig}^{k_3}(\boldsymbol{x}_{1i}) + \lambda_4 \boldsymbol{sig}^{k_4}(\boldsymbol{x}_{1i})\right)$.

Take the derivative of the sliding mode surface (32)

$$\begin{aligned}\dot{\boldsymbol{S}}_i &= \dot{\boldsymbol{x}}_{2i} + \frac{1}{N^2(\boldsymbol{x}_{1i})}\Big[N(\boldsymbol{x}_{1i})(\lambda_3\boldsymbol{P}_1 + \lambda_4\boldsymbol{P}_2)\boldsymbol{x}_{1i} - \dot{N}(\boldsymbol{x}_{1i})\Big(\lambda_3 \boldsymbol{sig}^{k_3}(\boldsymbol{x}_{1i}) + \lambda_4\boldsymbol{S}_{ci}\Big)\Big] \\ &= \boldsymbol{u}_i + \boldsymbol{d}_i - \hat{\boldsymbol{M}}_{\eta i}^{-1}(\boldsymbol{\eta}_i)\Big(\hat{\boldsymbol{C}}_{\eta i}(\boldsymbol{\eta}_i, \dot{\boldsymbol{\eta}}_i)\dot{\boldsymbol{\eta}}_i + \hat{\boldsymbol{D}}_{\eta i}(\boldsymbol{\eta}_i, \dot{\boldsymbol{\eta}}_i)\dot{\boldsymbol{\eta}}_i\Big) - \ddot{\boldsymbol{\eta}}_i^d \\ &+ \frac{1}{N^2(\boldsymbol{x}_{1i})}\Big[N(\boldsymbol{x}_{1i})(\lambda_3\boldsymbol{P}_1 + \lambda_4\boldsymbol{P}_2)\dot{\boldsymbol{x}}_{1i} - \dot{N}(\boldsymbol{x}_{1i})\Big(\lambda_3 \boldsymbol{sig}^{k_3}(\boldsymbol{x}_{1i}) + \lambda_4\boldsymbol{S}_{ci}\Big)\Big]\end{aligned} \tag{34}$$

Combining the disturbance observer Eq. (29) and the sliding-mode surface (32), a fixed-time formation controller is presented

$$\boldsymbol{u}_i = \boldsymbol{u}_{i1} + \boldsymbol{u}_{i2} \tag{35}$$

where

$$\boldsymbol{u}_{i1} = -\left(\begin{array}{c}\hat{\boldsymbol{d}}_i - \hat{\boldsymbol{M}}_{\eta i}^{-1}(\boldsymbol{\eta}_i)\Big(\hat{\boldsymbol{C}}_{\eta i}(\boldsymbol{\eta}_i, \dot{\boldsymbol{\eta}}_i)\dot{\boldsymbol{\eta}}_i + \hat{\boldsymbol{D}}_{\eta i}(\boldsymbol{\eta}_i, \dot{\boldsymbol{\eta}}_i)\dot{\boldsymbol{\eta}}_i\Big) - \ddot{\boldsymbol{\eta}}_i^d \\ + \frac{1}{N^2(\boldsymbol{x}_{1i})}\Big[N(\boldsymbol{x}_{1i})(\lambda_3\boldsymbol{P}_1 + \lambda_4\boldsymbol{P}_2)\dot{\boldsymbol{x}}_{1i} - \dot{N}(\boldsymbol{x}_{1i})\Big(\lambda_3 \boldsymbol{sig}^{k_3}(\boldsymbol{x}_{1i}) + \lambda_4\boldsymbol{S}_{ci}\Big)\Big]\end{array}\right) \tag{36}$$

$$\boldsymbol{u}_{i2} = -\frac{1}{N(\boldsymbol{S}_i)}\Big(\lambda_5 \boldsymbol{sig}^{k_5}(\boldsymbol{S}_i) + \lambda_6 \boldsymbol{sig}^{k_6}(\boldsymbol{S}_i)\Big) \tag{37}$$

where $N(\boldsymbol{S}_i) = a_3 + (1 - a_3)\exp\big(-b_3|\boldsymbol{S}_i|^{c_3}\big)$, $\begin{cases} c_3, & |\boldsymbol{S}_i| \geq 1 \\ 1, & |\boldsymbol{S}_i| < 1 \end{cases}$, $k_5 = 1 + \Big(\frac{m_3}{2n_3}\Big)(1 + \mathrm{sgn}(|\boldsymbol{S}_i| - 1))$, $k_6 = \frac{p_3}{q_3}$, $\lambda_5 > 0$, $\lambda_6 > 0$, $0 < a_3 < 1$, $b_3 > 0$, $c_3 > 0$, $m_3 > n_3 > 0$, $q_3 > p_3 > 0$ are four odd integers. $\boldsymbol{P}_2 = \begin{cases} k_4 \mathrm{diag}\big(|\boldsymbol{x}_{1i}|^{k_4 - 1}\big), \text{ if } \overline{\boldsymbol{S}}_i = 0 \text{ or } \overline{\boldsymbol{S}}_i \neq 0, \ |\boldsymbol{x}_{1i}| \geq \phi \\ \sigma_1 \boldsymbol{I}_3 + 2\sigma_2 \mathrm{diag}(|\boldsymbol{x}_{1i}|), \text{ if } \overline{\boldsymbol{S}}_i \neq 0, \ |\boldsymbol{x}_{1i}| < \phi \end{cases}$, $\boldsymbol{P}_1 = k_3 \mathrm{diag}\big(|\boldsymbol{x}_{1i}|^{k_3 - 1}\big)$.

Theorem 1. Applying the proposed controller (35) to the kinematics and dynamics Eq. (19), the formation errors can convergence to the origin with the settling time T satisfying $T < \max(T_0, T_1) + T_2$, where T_1 and T_2 are shown as

$$T_1 < \frac{1}{\lambda_5 \mu_3} + \frac{1}{\lambda_5(1 - \omega_3)} \ln\left(1 + \frac{\lambda_5}{2^{(\omega_3 - 1)/2}\lambda_6}\right) \tag{38}$$

$$T_2 < \frac{1}{\lambda_3 \mu_2} + \frac{1}{\lambda_3(1 - \omega_2)} \ln\left(1 + \frac{\lambda_3}{2^{(\omega_2 - 1)/2}\lambda_4}\right) \tag{39}$$

where $\mu_2 = \frac{m_2}{n_2}$, $\omega_2 = \frac{p_2}{q_2}$, $\mu_3 = \frac{m_3}{n_3}$, $\omega_3 = \frac{p_3}{q_3}$.

Proof. According to the characteristics of sliding-mode control, we divide the proof process into two parts.

Part 1. Substituting (35) into (34), we have

$$\dot{\boldsymbol{S}}_i = -\frac{1}{N(\boldsymbol{S}_i)}\Big(\lambda_5 \boldsymbol{sig}^{k_5}(\boldsymbol{S}_i) + \lambda_6 \boldsymbol{sig}^{k_6}(\boldsymbol{S}_i)\Big) + \boldsymbol{d}_i - \hat{\boldsymbol{d}}_i \tag{40}$$

Considering the Lyapunov function $V_2 = \frac{1}{2}\boldsymbol{S}_i^T \boldsymbol{S}_i$, we can get

$$\begin{aligned}\dot{V}_2 = \boldsymbol{S}_i^{\mathrm{T}}\dot{\boldsymbol{S}}_i &= -\boldsymbol{S}_i^{\mathrm{T}}\left(\frac{1}{N(\boldsymbol{S}_i)}\left(\lambda_5 \boldsymbol{sig}^{k_5}(\boldsymbol{S}_i) + \lambda_6 \boldsymbol{sig}^{k_6}(\boldsymbol{S}_i)\right) + \hat{\boldsymbol{d}}_i - \boldsymbol{d}_i\right) \\ &\le -\frac{1}{N(\boldsymbol{S}_i)}\sum_{j=1}^{3}\left(\lambda_5\left|\boldsymbol{S}_{i,j}\right|^{k_5+1} + \lambda_6\left|\boldsymbol{S}_{i,j}\right|^{k_6+1}\right) - \boldsymbol{S}_i^{\mathrm{T}}\boldsymbol{d}_e \\ &\le -\frac{1}{N(\boldsymbol{S}_i)}\lambda_5(2V_2)^{(k_5+1)/2} - \frac{1}{N(\boldsymbol{S}_i)}\lambda_6(2V_2)^{(k_6+1)/2}\end{aligned} \tag{41}$$

when $|\boldsymbol{S}_i| \ge 1$, one has

$$\dot{V}_2 \le -\frac{1}{N(\boldsymbol{S}_i)}\lambda_5(2V_2)^{(\mu_3+1)/2} - \frac{1}{N(\boldsymbol{S}_i)}\lambda_6(2V_2) \tag{42}$$

when $|\boldsymbol{S}_i| < 1$, we can obtain

$$\dot{V}_2 \le -\frac{1}{N(\boldsymbol{S}_i)}\lambda_5(2V_2) - \frac{1}{N(\boldsymbol{S}_i)}\lambda_6(2V_2)^{(\omega_3+1)/2} \tag{43}$$

Applying Lemma 1 and (41), we have $V_2 = 0$. According to Lemma 3, we have $\tilde{\boldsymbol{d}}_i = 0$ when $t \ge T_0$. Therefore, the proposed sliding-mode surface can converge to the origin when $t \ge \max(T_0,\ T_1)$, and the fixed time T_1 satisfies

$$T_1 < \frac{1}{\lambda_5\mu_3} + \frac{1}{\lambda_5(1-\omega_3)}\ln\left(1 + \frac{\lambda_5}{2^{(\omega_3-1)/2}\lambda_6}\right) \tag{44}$$

Part 2. When the sliding-mode surface reaches $\boldsymbol{S}_i = 0$, we have

$$\boldsymbol{S}_i = \boldsymbol{x}_{2i} + \frac{1}{N(\boldsymbol{x}_{1i})}\left(\lambda_3 \boldsymbol{sig}^{k_3}(\boldsymbol{x}_{1i}) + \lambda_4 \boldsymbol{sig}^{k_4}(\boldsymbol{x}_{1i})\right) = 0 \tag{45}$$

Considering the Lyapunov function $V_3 = \frac{1}{2}\boldsymbol{x}_{1i}^{\mathrm{T}}\boldsymbol{x}_{1i}$, we can get

$$\begin{aligned}\dot{V}_3 = \boldsymbol{x}_{1i}^{\mathrm{T}}\dot{\boldsymbol{x}}_{1i} &= \boldsymbol{x}_{1i}^{\mathrm{T}}\dot{\boldsymbol{x}}_{2i} = -\boldsymbol{x}_{1i}^{\mathrm{T}}\frac{1}{N(\boldsymbol{x}_{1i})}\left(\lambda_3 \boldsymbol{sig}^{k_3}(\boldsymbol{x}_{1i}) + \lambda_4 \boldsymbol{sig}^{k_4}(\boldsymbol{x}_{1i})\right) \\ &\le -\frac{1}{N\left(\boldsymbol{x}_{1i,J}\right)}\sum_{i=1}^{3}\left(\lambda_3\left|\boldsymbol{x}_{1i,J}\right|^{k_3+1} + \lambda_4\left|\boldsymbol{x}_{1i,J}\right|^{k_4+1}\right) \\ &\le -\frac{1}{N(\boldsymbol{x}_{1i})}\lambda_3(2V_3)^{(k_3+1)/2} - \frac{1}{N(\boldsymbol{x}_{1i})}\lambda_4(2V_3)^{(k_4+1)/2}\end{aligned} \tag{46}$$

when $|\boldsymbol{x}_{1i}| \ge 1$, one has

$$\dot{V}_3 \le -\frac{1}{N(\boldsymbol{x}_{1i})}\lambda_3(2V_3)^{(\mu_2+1)/2} - \frac{1}{N(\boldsymbol{x}_{1i})}\lambda_4(2V_3) \tag{47}$$

when $|\boldsymbol{x}_{1i}| < 1$, we can obtain

$$\dot{V}_3 \le -\frac{1}{N(\boldsymbol{x}_{1i})}\lambda_3(2V_3) - \frac{1}{N(\boldsymbol{x}_{1i})}\lambda_4(2V_3)^{(\omega_2+1)/2} \tag{48}$$

Similarly, according to Lemma 1, it is shown that the system state can converge to $R = \left\{(\boldsymbol{x}_{1i},\ \boldsymbol{x}_{2i}) : \left|\boldsymbol{x}_{1i,j}\right| \le \phi,\ \left|\boldsymbol{x}_{2i,j}\right| \le \frac{1}{N(\boldsymbol{x}_{1i})}\lambda_3\phi^{k_3} + \frac{1}{N(\boldsymbol{x}_{1i})}\lambda_4\phi^{k_4}\right\}$ in a fixed time T_2, and the convergence time T_2 satisfies

$$T_2 < \frac{1}{\lambda_3\mu_2} + \frac{1}{\lambda_3(1-\omega_2)}\ln\left(1 + \frac{\lambda_3}{2^{(\omega_2-1)/2}\lambda_4}\right) \tag{49}$$

The proof is completed.

Remark 3. The proposed control method has superior performance in this paper. It not only expedites the convergence rate of the whole system, but also improves the robustness of the system, which has a certain guiding significance for practical application. Moreover, the control method also has certain universality. For example, it can be applied to the control field of unmanned aerial vehicle. The difference between the two control objects is the difference of the models. We can apply it to the unmanned aerial vehicle as long as we make some adjustments to the proposed method.

4 Simulation Studies

To demonstrate the feasibility of the proposed controller method, the simulation study is conducted. The model parameter matrices are shown in [36]. The external disturbances $\hat{\boldsymbol{M}}_{\eta i}^{-1}(\boldsymbol{\eta}_i)\boldsymbol{R}(\psi_i)\boldsymbol{\tau}_{di} = [2\sin(0.1t),\ 1.5\sin(0.2t),\ \sin(0.05t)]^{\mathrm{T}}$ and 20% uncertainties of the model parameters are taken into account. The control parameters are selected as $a = 0.1, b = 2.5, c = 3.5, \gamma_1 = 2, \gamma_2 = \gamma_3 = 6, \lambda_1 = \lambda_2 = \lambda_3 = 0.01, \lambda_2 = \lambda_4 = \lambda_6 = 2, m_1 = m_2 = m_3 = 35, n_1 = n_2 = n_3 = 33, \phi = 0.001, p_1 = p_2 = p_3 = 9, q_1 = q_2 = q_3 = 15, a_1 = a_2 = a_3 = 0.8, b_1 = b_2 = b_3 = 10, c_1 = c_2 = c_3 = 2$. The initial values of AUV1 and AUV2 are chosen as $\boldsymbol{\eta}_1 = [-4,\ 3,\ 2]^{\mathrm{T}}$, $\boldsymbol{v}_1 = [0,\ 0,\ 0]^{\mathrm{T}}$, $\boldsymbol{\eta}_2 = [-4,\ -3,\ 2]^{\mathrm{T}}$, $\boldsymbol{v}_2 = [0,\ 0,\ 0]^{\mathrm{T}}$. The reference trajectory of the global leader is selected as $\boldsymbol{\eta}_l = [0.1t,\ 2\cos(0.1t) - 2,\ 0.01t + 2.5]^{\mathrm{T}}$. The faults parameters are designed as $e_1 = \begin{cases} 1\ t \le 30 \\ 1.2\ \text{otherwise} \end{cases}$, $e_2 = \begin{cases} 1\ t \le 28 \\ 1.15\ \text{otherwise} \end{cases}$, $e_3 = \begin{cases} 1\ t \le 20 \\ 0.9\ \text{otherwise} \end{cases}$, $\overline{\boldsymbol{\tau}}_i = [0.3,\ 0.4,\ 0.2]^{\mathrm{T}}$. For any initial velocity $\boldsymbol{v}_i = \boldsymbol{R}^{-1}\boldsymbol{\omega}_i$, and three different initial values are considered. Case 1: $\boldsymbol{\eta}_1 = [-4,\ 3,\ 2]^{\mathrm{T}}, \boldsymbol{\omega}_1 = [0,\ 0,\ 0]^{\mathrm{T}}, \boldsymbol{\eta}_2 = [-4,\ -3,\ 2]^{\mathrm{T}}, \boldsymbol{\omega}_2 = [0,\ 0,\ 0]^{\mathrm{T}}$. Case 2: $\boldsymbol{\eta}_1 = [-8,\ 2,\ 1.5]^{\mathrm{T}}$, $\boldsymbol{\omega}_1 = [0.01,\ 0.02,\ 0]^{\mathrm{T}}$, $\boldsymbol{\eta}_2 = [-8,\ -2,\ 1.5]^{\mathrm{T}}$, $\boldsymbol{\omega}_2 = [0.02,\ 0.02,\ 0]^{\mathrm{T}}$. Case 3: $\boldsymbol{\eta}_1 = [-6,\ 1,\ 1]^{\mathrm{T}}$, $\boldsymbol{\omega}_1 = [0.03,\ -0.01,\ 0.01]^{\mathrm{T}}$, $\boldsymbol{\eta}_2 = [-6,\ -1,\ 1]^{\mathrm{T}}, \boldsymbol{\omega}_2 = [0.02,\ -0.02,\ 0.01]^{\mathrm{T}}$.

Consider a formation configuration consisting of three AUVs, which are represented as "AUV1", "AUV2" and "AUV3", respectively. AUV3 acts as the leader to provide the desired trajectory information. Figure 1 shows the communication topology. The desired formation structure of AUVs is an isosceles triangle. The formation trajectories of three AUVs on the horizontal plane are shown in Fig. 2. It is obvious that the desired isosceles triangle formation configuration is achieved. The distances between AUV1 & AUV3 and AUV2 & AUV3 are shown in Fig. 3. The results show that the distance between the leader-follower members is 4m, which can be changed by adjusting the parameters of potential field function. Figures 4–7 demonstrate the convergence characteristics of the

proposed control method under different initial states. It can be seen that the convergence time of the proposed algorithm is fixed and not limited by the initial state. The errors of position and velocity and the control input are shown in Figs. 8–10. It can be shown that the errors can converge to the origin in a fixed time. The composite disturbances and its estimation are shown in Figs. 11 and 12. It can be seen that the designed disturbance observer can accurately estimate the composite disturbances, which enhances the robustness of the system.

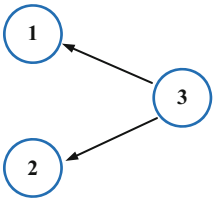

Fig. 1. Communication topology

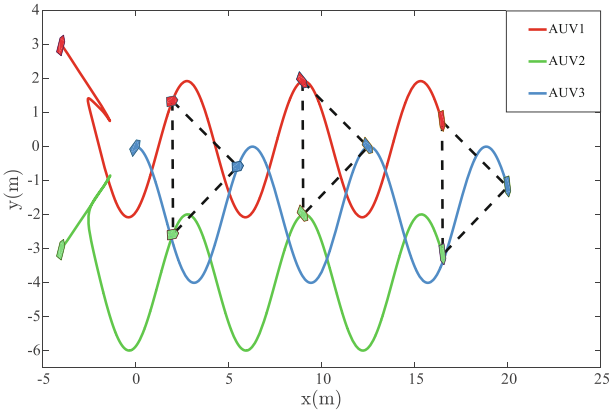

Fig. 2. Formation trajectories in the horizontal plane

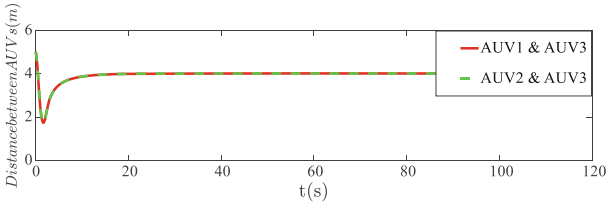

Fig. 3. Distance between the AUVs

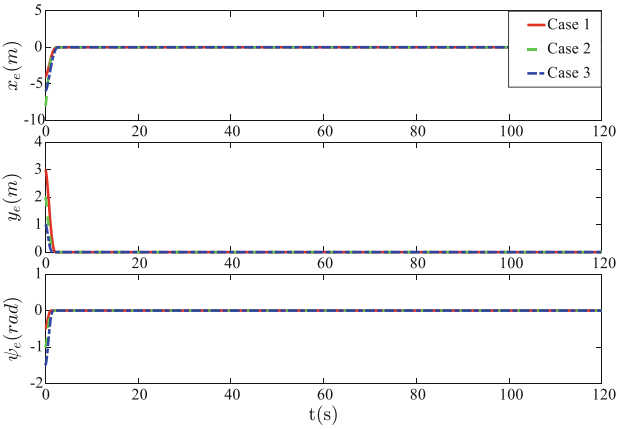

Fig. 4. Position errors of AUV1 under different initial conditions

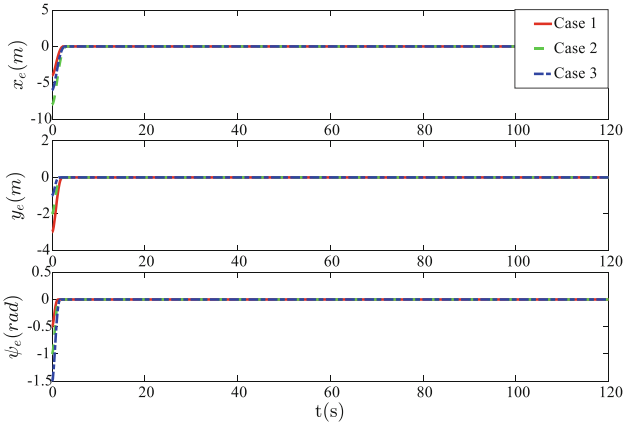

Fig. 5. Position errors of AUV2 under different initial conditions

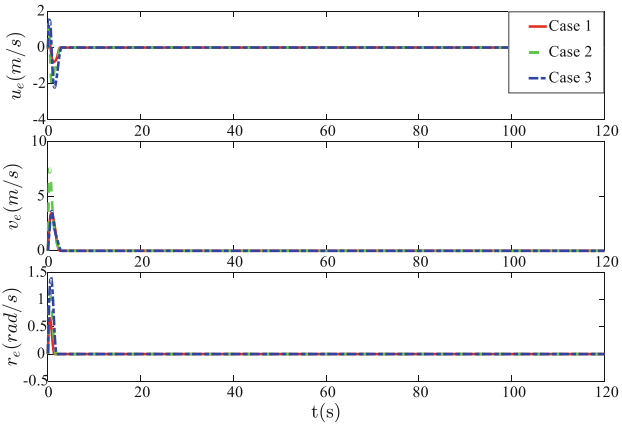

Fig. 6. Velocity errors of AUV1 under different initial conditions

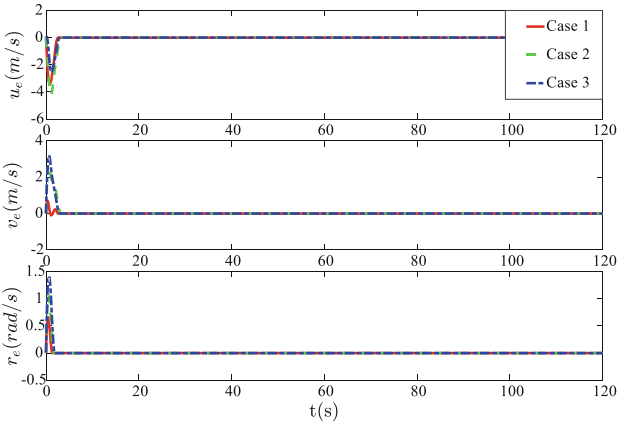

Fig. 7. Velocity errors of AUV2 under different initial conditions

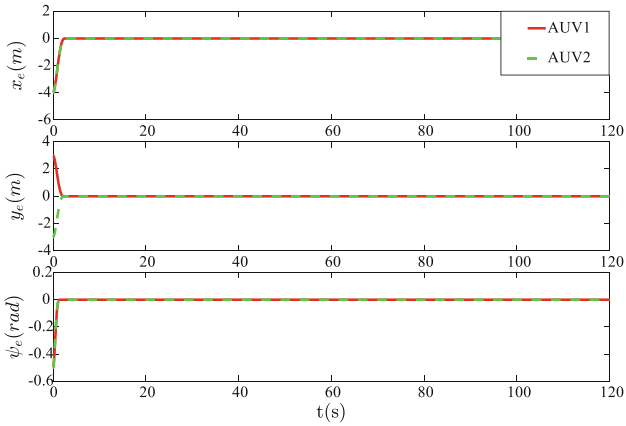

Fig. 8. Position errors of AUV1 and AUV2

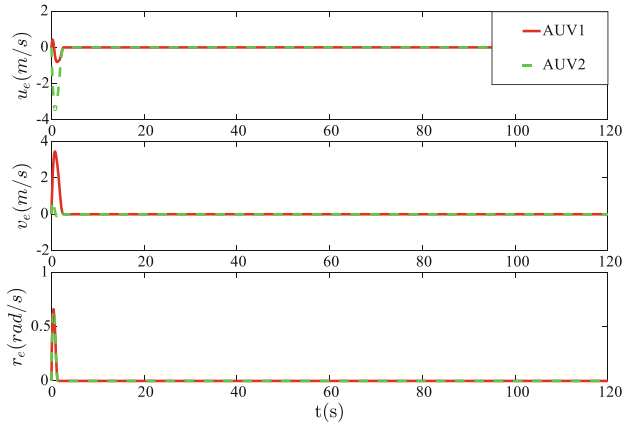

Fig. 9. Velocity errors of AUV1 and AUV2

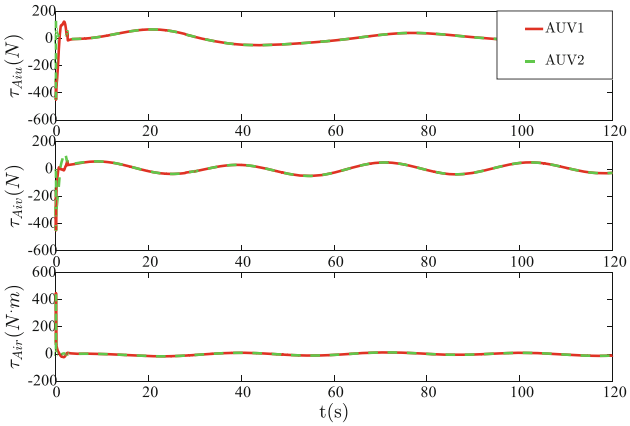

Fig. 10. Control inputs of AUV1 and AUV2

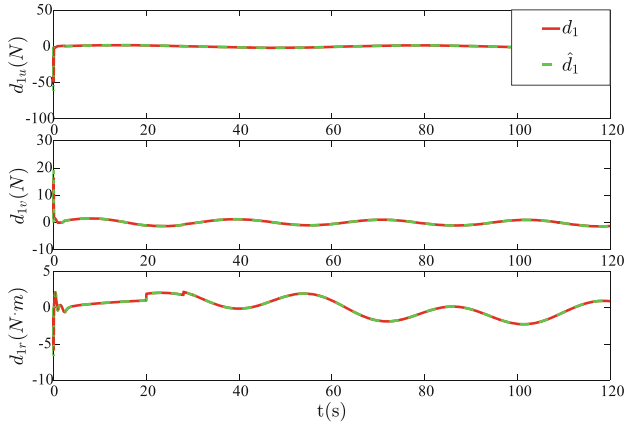

Fig. 11. The disturbance estimations of AUV1

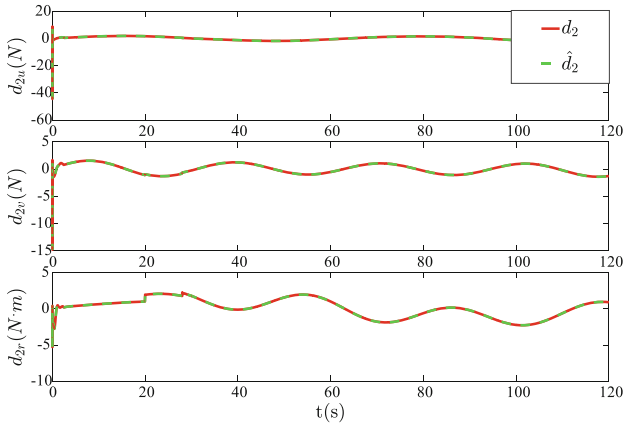

Fig. 12. The disturbance estimations of AUV2

5 Conclusion

In this paper, considering the problem of actuator faults, model uncertainties and unknown disturbances, a fast fixed-time formation control method is proposed. Specifically, the desired formation configuration can be obtained by properly adjusting the parameters of the artificial potential field function. Then, a fixed-time disturbance observer is designed for composite disturbances. Further, by combining disturbance observer and fast nonsingular terminal sliding-mode surface, a formation control method is designed. Eventually, the advantages and effectiveness of this method is verified by simulation.

References

1. Wang, N., Zhang, Y., Ahn, C., Xu, Q.: Autonomous pilot of unmanned surface vehicles: Bridging path planning and tracking. IEEE Trans. Veh. Technol. **71**(3), 2358–2374 (2022)
2. Gao, L., Qin, H., Li, P.: Disturbance observer-based finite-time exact bottom-following control for a BUV with input saturation. Ocean Eng. **266**, 112650 (2022)
3. Wang, N., Er, M., Sun, J., Liu, Y.: Adaptive robust online constructive fuzzy control of a complex surface vehicle system. IEEE Trans. Cybern. **46**(7), 1511–1523 (2016)
4. Cui, R., Shuzhi, S., Bernard, V., Yoo, S.: Leader–follower formation control of underactuated autonomous underwater vehicles. Ocean Eng. **37**(17), 1491–1502 (2010)
5. Balch, T., Arkin, R.: Behavior-based formation control for multirobot teams. IEEE Trans. Robot. Autom. **14**(6), 926–939 (1998)
6. Pashna, M., Yusof, R., Ismail, Z., Namerikawa, T., Yazdani, S.: Autonomous multi-robot tracking system for oil spills on sea surface based on hybrid fuzzy distribution and potential field approach. Ocean Eng. **207**, 107238 (2020)
7. Do, K.: Formation control of multiple elliptical agents with limited sensing ranges. Automatica **48**(7), 1330–1338 (2012)
8. Peng, Z., Wang, J., Wang, D.: Distributed containment maneuvering of multiple marine vessels via neurodynamics-based output feedback. IEEE Trans. Industr. Electr. **64**, 3831–3839 (2017)

9. Xu, J.: Fault tolerant finite-time leader–follower formation control for autonomous surface vessels with LOS range and angle constraints. Automatica **68**, 228–236 (2016)
10. Wu, T., Xue, K., Wang, P.: Leader-follower formation control of USVs using APF-based adaptive fuzzy logic nonsingular terminal sliding mode control method. J. Mech. Sci. Technol. **36**, 1–12 (2022). https://doi.org/10.1007/s12206-022-0336-y
11. Wang, N., Ahn, C.: Coordinated trajectory tracking control of a marine aerial-surface heterogeneous system. IEEE/ASME Trans. Mechatron. **26**(6), 3198–3210 (2021)
12. Yang, L., Yang, J.: Nonsingular fast terminal sliding-mode control for nonlinear dynamical systems. Int. J. Robust Nonlinear Control **21**(16), 1865–1879 (2011)
13. Wang, N., Karimi, H., Li, H., Su, S.: Accurate trajectory tracking of disturbed surface vehicles: a finite-time control approach. IEEE/ASME Trans. Mechatron. **24**(3), 1064–1074 (2019)
14. Chen, M., Shi, P., Lim, C.: Robust constrained control for MIMO nonlinear systems based on disturbance observer. IEEE Trans. Autom. Control **60**(12), 3281–3286 (2015)
15. Wang, N., Er, M.: Self-constructing adaptive robust fuzzy neural tracking control of surface vehicles with uncertainties and unknown disturbances. IEEE Trans. Control Syst. Technol. **23**(3), 991–1002 (2015)
16. Qiao, L., Bowen, Y., Wu, D., Zhang, W.: Design of three exponentially convergent robust controllers for the trajectory tracking of autonomous underwater vehicles. Ocean Eng. **134**, 157–172 (2017)
17. Qiao, L., Zhang, W.: Adaptive second-order fast nonsingular terminal sliding mode tracking control for fully actuated autonomous underwater vehicles. IEEE J. Oceanic Eng. **44**(2), 363–385 (2019)
18. Qiao, L., Zhang, W.: Trajectory tracking control of AUVs via adaptive fast nonsingular integral terminal sliding mode control. IEEE Trans. Industr. Inform. **16**(2), 1248–1258 (2020)
19. Wang, N., Su, S.: Finite-time unknown observer based interactive trajectory tracking control of asymmetric underactuated surface vehicles. IEEE Trans. Control Syst. Technol. **29**(2), 794–803 (2021)
20. Polyakov, A.: Nonlinear feedback design for fixed-time stabilization of linear control systems. IEEE Trans. Autom. Control **57**(8), 2106–2110 (2012)
21. Wang, C., Tnunay, H., Zuo, Z., Lennox, B., Ding, Z.: Fixed-time formation control of multirobot systems: design and experiments. IEEE Trans. Industr. Electron. **66**(8), 6292–6301 (2019)
22. Wang, N., Er, M.: Direct Adaptive fuzzy tracking control of marine vehicles with fully unknown parametric dynamics and uncertainties. IEEE Trans. Control Syst. Technol. **24**(5), 1845–1852 (2016)
23. Du, H., Wen, G., Wu, D., Cheng, Y., Lü, J.: Distributed fixed-time consensus for nonlinear heterogeneous multi-agent systems. Automatica **113**, 108797 (2020)
24. Wang, N., Gao, Y., Zhang, X.: Data-driven performance-prescribed reinforcement learning control of an unmanned surface vehicle. IEEE Trans. Neural Netw. Learn. Syst. **32**(12), 5456–5467 (2021)
25. Van, M.: An enhanced tracking control of marine surface vessels based on adaptive integral sliding mode control and disturbance observer. ISA Trans. **90**, 30–40 (2019)
26. Weng, Y., Wang, N.: Finite-time observer-based model-free time-varying sliding-mode control of disturbed surface vessels. Ocean Eng. **251**, 110866 (2022)
27. Wang, N., Qian, C., Sun, J., Liu, Y.: Adaptive robust finite-time trajectory tracking control of fully actuated marine surface vehicles. IEEE Trans. Control Syst. Technol. **24**(4), 1454–1462 (2016)
28. Lee, J., Chang, P., Jin, M.: Adaptive integral sliding mode control with time-delay estimation for robot manipulators. IEEE Trans. Industr. Electron. **64**(8), 6796–6804 (2017)
29. Weng, Y., Wang, N., Carlos, G.: Data-driven sideslip observer-based adaptive sliding-mode path-following control of underactuated marine vessels. Ocean Eng. **197**, 106910 (2020)

30. Cui, R., Chen, L., Yang, C., Chen, M.: Extended state observer-based integral sliding mode control for an underwater robot with unknown disturbances and uncertain nonlinearities. IEEE Trans. Industr. Electron. **64**(8), 6785–6795 (2017)
31. Kim, J., Joe, H., Yu, S., Lee, J., Kim, M.: Time-delay controller design for position control of autonomous underwater vehicle under disturbances. IEEE Trans. Industr. Electron. **63**(2), 1052–1061 (2016)
32. Wang, N., Gao, Y., Zhao, H., Ahn, C.: Reinforcement learning-based optimal tracking control of an unknown unmanned surface vehicle. IEEE Trans. Neural Netw. Learn. Syst. **32**(7), 3034–3045 (2021)
33. Guo, G., Zhang, P.: Asymptotic stabilization of USVs with actuator dead-zones and yaw constraints based on fixed-time disturbance observer. IEEE Trans. Veh. Technol. **69**(1), 302–316 (2020)
34. Wu, Y., Wang, Z., Huang, Z.: Distributed fault detection for nonlinear multi-agent systems under fixed-time observer. J. Franklin Inst. **356**(13), 7515–7532 (2019)
35. Cao, L., Xiao, B., Golestani, M., Ran, D.: Faster fixed-time control of flexible spacecraft attitude stabilization. IEEE Trans. Industr. Inform. **16**(2), 1281–1290 (2020)
36. Do, K., Pan, J.: Global robust adaptive path following of underactuated ships. Automatica **42**(10), 1713–1722 (2006)